

# Tau Tridents at Accelerator Neutrino Facilities

Innes Bigaran,<sup>1,2,\*</sup> P. S. Bhupal Dev,<sup>3,†</sup> Diego Lopez Gutierrez,<sup>3,‡</sup> and Pedro A. N. Machado<sup>2,§</sup>

<sup>1</sup>*Department of Physics & Astronomy, Northwestern University, 2145 Sheridan Road, Evanston, IL 60208, USA*

<sup>2</sup>*Theoretical Physics Department, Fermilab, P.O. Box 500, Batavia, IL 60510, USA*

<sup>3</sup>*Department of Physics and McDonnell Center for the Space Sciences, Washington University, St. Louis, MO 63130, USA*

We present the first detailed study of Standard Model (SM) neutrino tridents involving tau leptons at the near detectors of accelerator neutrino facilities. These processes were previously thought to be negligible, even at future facilities like DUNE, based on approximations that underestimated the tau trident cross sections. Our full  $2 \rightarrow 4$  calculation, including both coherent and incoherent scatterings, reveals that the DUNE near detector will actually get a non-negligible number of tau tridents, which is an important background to new physics searches. We identify promising kinematic features that may allow distinction of tau tridents from the usual neutrino charged-current background at DUNE, and thus could establish the observation of tau tridents for the first time. We also comment on the detection prospects at other accelerator and collider neutrino experiments.

## I. INTRODUCTION

The origin of neutrino flavor-oscillations, and thus neutrino masses, remains one of the greatest unsolved problems with the Standard Model (SM) of particle physics. In order to reconcile the empirical evidence of nonzero neutrino masses with the SM, a detailed study of the physics of the neutrino sector is imperative. A drawback of neutrino interaction studies is the weak interaction strengths of neutrinos with other SM particles, necessitating experimental programs with extraordinarily large statistics. The next-generation accelerator-neutrino experiments at the Intensity Frontier, such as DUNE [1] and T2HK [2], are poised to shed light on the neutrino sector in unprecedented ways, unveiling further information about the interactions of SM neutrinos and perhaps yielding a portal to physics beyond the SM (BSM).

Of all SM particle species, the interactions of the tau neutrino ( $\nu_\tau$ ) remain the least well-studied. The low cross sections for interactions, high tau-production thresholds and experimental difficulty to distinguish it from other neutrino states make studies of  $\nu_\tau$  extraordinarily difficult. To date, the global dataset of directly observed  $\nu_\tau$  interactions consists of only  $\mathcal{O}(10)$  events at DONuT [3] and OPERA [4], making a future  $\nu_\tau$  observation highly significant and a key target for the accelerator-neutrino programs.

Even more challenging than simply observing  $\nu_\tau$  charged-current (CC) interaction is to study neutrino trident production involving taus. Neutrino tridents are SM processes involving the creation of a charged-lepton pair via an energetic neutrino scattering with a nucleus,  $\nu_\ell N \rightarrow \nu_\ell \ell \ell' N$  [5] (see Fig. 1). Although rare, these processes provide a precision test of the SM weak sector [6],

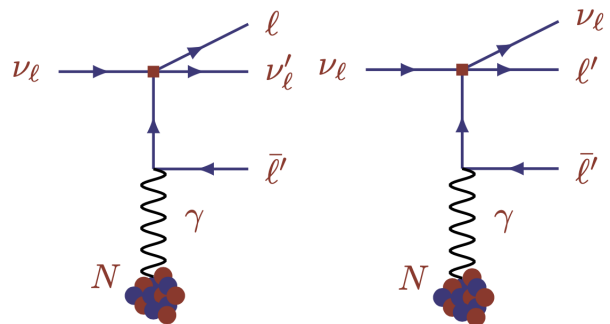


FIG. 1. Neutrino trident production via charged- (left) and neutral-current (right) four-fermion interactions in the SM.

as they are affected by both  $W$  and  $Z$ -mediated interactions. They are also relevant for BSM physics searches, and in particular, tridents with  $\ell \neq \ell'$  will be an important background for charged lepton-flavor violation searches (see e.g., Refs. [7–12]). So far, only the dimuon trident  $\nu_\mu N \rightarrow \nu_\mu \mu^+ \mu^- N$  has been observed at  $\sim 3\sigma$  level by CHARM [13] and CCFR [14] experiments (see also NuTeV [15, 16]) while the other  $\ell \ell'$  final states have never been observed. This has motivated new proposals for observing tridents using future accelerator [17–19] and collider [20, 21] neutrino experiments, as well as at neutrino telescopes [22, 23]. Typically in the literature, studies have focused on the electron and muon tridents due to their relatively smaller energy threshold. The few existing studies [17, 24, 25] which briefly mentioned tau tridents have highlighted their low likelihood in standard accelerator-neutrino setups originating from  $\nu_\mu$  scattering, particularly at near detectors.

One key challenge for both  $\nu_\tau$  CC interactions and tau tridents is the reconstruction of the tau lepton. One way to achieve this is by having excellent spatial resolution, at the micrometer level or below, which is typically attained using emulsion detectors such as FASER $\nu$  [26]. This al-

\* [ibigaran@fnal.gov](mailto:ibigaran@fnal.gov)

† [bdev@wustl.edu](mailto:bdev@wustl.edu)

‡ [d.lopezgutierrez@wustl.edu](mailto:d.lopezgutierrez@wustl.edu)

§ [pmachado@fnal.gov](mailto:pmachado@fnal.gov)

lows to observe the vertex displacement from the tau propagation. Alternatively, detailed event reconstruction capabilities, as is the case for Liquid Argon Time Projection Chambers (LArTPCs) such as in DUNE [1], may allow for excellent signal-to-background ratios even if the displaced vertex from tau decay is not observed [27, 28].

In this paper, we make the first detailed study of neutrino tridents involving one or two tau leptons at neutrino accelerator facilities, focusing specifically on DUNE Near Detector (ND) [29], at which the tau tridents were neglected in previous studies. We consider the DUNE standard CP-optimized flux, as well as the tau-optimized flux [30], for our calculation. We find non-negligible number of tau tridents at DUNE ND in both cases, and especially so in the tau-optimized mode. The prospective detection of these events is promising due to low intrinsic tau neutrino background and significantly different kinematic distributions between the tau trident signal and  $\nu_\mu$  CC backgrounds. In the Appendix, we comment on trident events at current accelerator neutrino facilities and collider neutrino experiments.

## II. NEUTRINO TRIDENT CROSS SECTION

Neutrino tridents are exceptionally rare  $2 \rightarrow 4$  electroweak scattering processes in the SM [5]. There are two key regimes to consider for tridents: the coherent scattering of neutrinos off nuclei without resolving their substructure, and the incoherent or diffractive scattering of neutrinos off individual nucleons. Coherent scattering cross sections are expected to dominate so long as the momentum transfer  $Q$  is significantly lower than the inverse-nuclear radius [5]. For larger  $Q$ , incoherent interactions become relevant where the leptons interact with individual nucleons, and at still larger  $Q$  (deep) inelastic interactions with quarks will become relevant. As shown in Refs. [17, 25], the inelastic contribution to trident production is negligible (at most 1%) in the energy range of our interest.

Kinematically, the flavor structure of neutrino tridents is limited by the mass-hierarchy of charged-leptons. Conservation of momentum and energy yields a threshold of initial neutrino energy for the production of a trident:

$$E_\nu^{\text{th}} \approx \frac{(m_\ell + m'_\ell + M_{\text{tgt}})^2 - M_{\text{tgt}}^2}{2M_{\text{tgt}}}, \quad (1)$$

where for incoherent scattering  $M_{\text{tgt}} = M_N$  is the nucleon mass ( $\sim 1$  GeV), and for coherent scattering  $M_{\text{tgt}} = M$  is the nuclear mass which may lead to an enhancement of the latter scattering regime. The threshold for various trident channels are listed in Table I for three different nuclei, namely, Argon, Tungsten and Iron, which are respectively the detector materials for DUNE and FASER $\nu$ , as well as T2K and MINOS near detectors. The larger tau mass increases the energy threshold and reduces the likelihood of tau-production via the trident, but it remains possible if the neutrino energy

TRIDENT PROCESS	$E_\nu^{\text{th}}$ (GeV)			
	INCOHERENT (proton)	COHERENT		
		$^{40}\text{Ar}$	$^{184}\text{W}$	$^{56}\text{Fe}$
$\nu_i N \rightarrow \nu_i N e^+ e^-$	0.001	0.001	0.001	0.001
$\nu_i N \rightarrow \nu_i N \mu^+ \mu^-$	0.24	0.21	0.21	0.21
$\nu_i N \rightarrow \nu_i N \tau^+ \tau^-$	10	3.7	3.6	3.7
$\nu_\mu N \rightarrow \nu_e N e^- \mu^+$	0.11	0.11	0.11	0.11
$\nu_\mu N \rightarrow \nu_\tau N \tau^- \mu^+$	3.8	1.9	1.9	1.9
$\nu_e N \rightarrow \nu_\tau N \tau^- e^+$	3.5	1.8	1.8	1.8

TABLE I. Threshold energies for various neutrino trident channels. For incoherent scattering, we utilize the proton mass as a proxy for the mean nucleon mass.

reaches above threshold. Moreover, incoherent scattering for tau tridents has a much higher threshold than coherent scattering, unlike the electron and muon tridents, where both processes have similar thresholds since  $m_{e,\mu}/M_N, m_{e,\mu}/M \ll 1$ .

In both processes shown in Fig. 1, the neutrino interactions with  $W$  or  $Z$  give rise to two charged leptons, which then couple to the nucleus. Estimating the hadronic current has significant uncertainties, though it is independent of whether CC or NC interactions are generating the leptonic current in the trident process. Below  $10^8$  GeV, the hadronic contributions arising from virtual weak boson-nucleus interactions and from mixing with the photon are negligible [25].

Both coherent and incoherent scattering processes considered here involve elastic scattering of the neutrino off the target. The former is described by a nuclear form-factor, and the latter by a nucleon form factor. The cross sections may be calculated using [18]

$$\frac{d\sigma_{\nu X}}{dQ^2 d\hat{s}} = \frac{1}{32\pi^2} \frac{1}{\hat{s}Q^2} [h_X^T(Q^2, \hat{s})\sigma_{\nu\gamma}^T(Q^2, \hat{s}) + h_X^L(Q^2, \hat{s})\sigma_{\nu\gamma}^L(Q^2, \hat{s})], \quad (2)$$

where  $X = c, i$  denote the coherent and incoherent scattering regimes, respectively.  $Q^2 = -q^2$  is the photon virtuality, and  $\hat{s} \equiv Q^2 + (k_1 + q)^2$ , where  $k_1$  is the four-momentum of the incoming neutrino. Eq. (2) factorizes the contributions to the trident process into transverse ( $T$ ) and longitudinal ( $L$ ) hadronic ( $h_X^{L/T}$ ) and leptonic ( $\sigma_{\nu\gamma}^{L/T}$ ) components. The functions  $h_X^{L/T}$  are dimensionless flux factors including the nuclear/nucleon form-factors  $F(Q^2)/H(Q^2)$ , discussed in Appendix A. For the incoherent contribution to the cross section, Eq. (2) is further multiplied by a Pauli-blocking factor, derived by modeling the nucleus as an ideal Fermi Gas, assuming equal density of protons and neutrons [31],

$$\Theta(|\vec{q}|) = \begin{cases} \frac{3}{2} \frac{|\vec{q}|}{2k_F} - \frac{1}{2} \left( \frac{|\vec{q}|}{2k_F} \right)^3 & \text{for } |\vec{q}| < 2k_F \\ 1 & \text{for } |\vec{q}| \geq 2k_F \end{cases}, \quad (3)$$

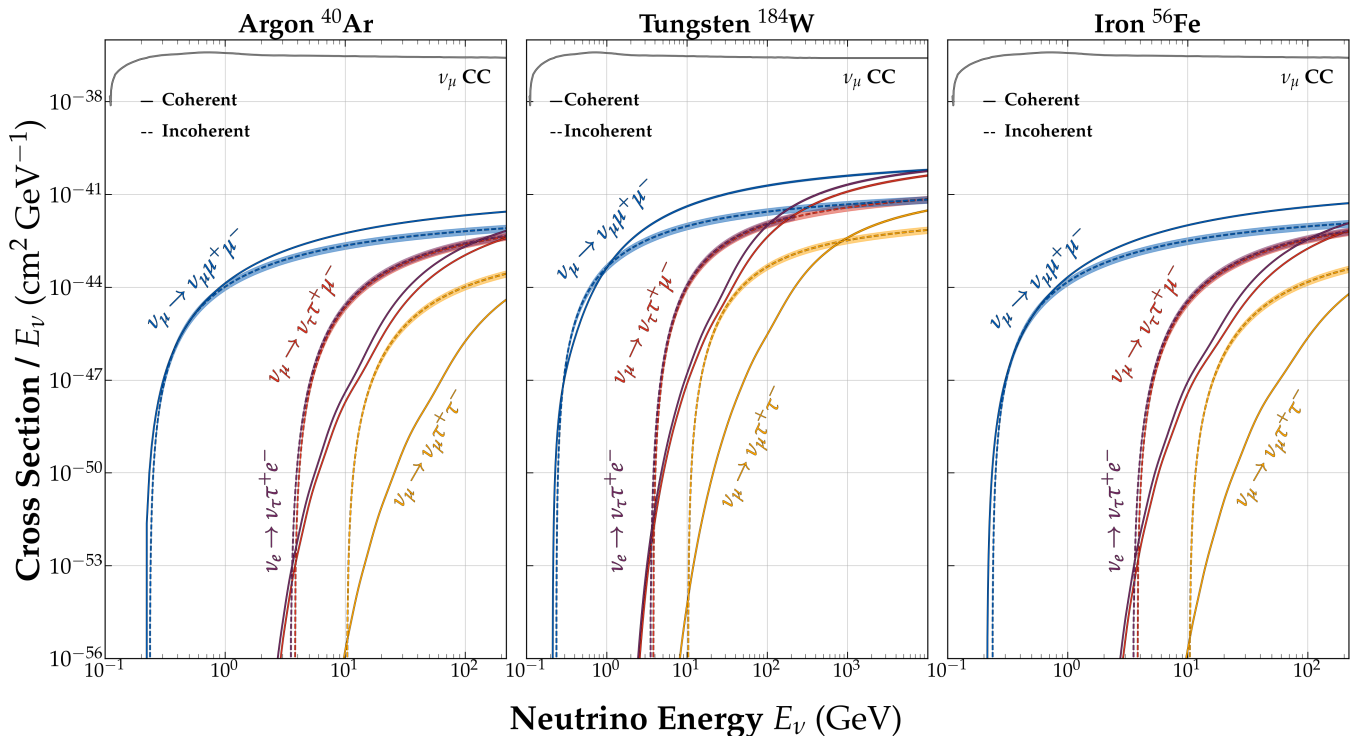


FIG. 2. Neutrino trident cross sections on different targets: Argon (left), Tungsten (middle) and Iron (right). Note that  $\nu_\mu \rightarrow \nu_\tau \tau^+ \mu^-$  and  $\nu_e \rightarrow \nu_\tau \tau^+ e^-$  have significant overlap but both are shown here for completeness. The  $\nu_\mu$  CC cross section is also shown for comparison. The antineutrino cross sections are the same as for neutrinos.

where  $\vec{q}$  is the spatial component of the momentum transfer to the nucleus, and  $k_F$  is the Fermi momentum of the gas, taken to be  $k_F = 235$  MeV. The leptonic components are calculated as cross sections between a neutrino and an off-shell photon,

$$\sigma_{\nu\gamma}^{L/T} = \frac{1}{2(k_1 + q)^2} \int d\text{PS}_3 \frac{1}{2} \sum_{\text{spins}} |\mathcal{M}_{\nu\gamma}^{L/T}|^2, \quad (4)$$

where  $d\text{PS}_3$  is the Lorentz invariant three-body phase space, and  $\frac{1}{2} \sum_{\text{spins}} |\mathcal{M}_{\nu\gamma}^{L/T}|^2$  is the spin-averaged matrix element for  $\nu_\ell + \gamma_{L/T} \rightarrow \nu_{\ell'} + \ell' + \ell$ , with a longitudinal or transversely polarized photon.

Here we remark on an alternative approach for calculating this  $\sigma_{\nu\gamma}$  component of the cross section, utilizing the equivalent photon approximation (EPA) [32]. To date, the only tau trident estimates for DUNE are given in Ref. [17], which employed the EPA, and deemed these processes inaccessible at DUNE energies. In the EPA, the infrared pole of the propagator for on-shell photon exchange between the lepton and nucleus is assumed to yield a dominant contribution to the cross section. As  $Q^2 \rightarrow 0$ , the transverse cross section approaches that of an on-shell photon, and the longitudinal component vanishes. Thus, when applying the EPA the longitudinal contributions in Eq. (2) are omitted, and the total cross section scales roughly as  $\sigma \sim G_F^2 E_\nu Q_{\text{max}} \log[E_\nu Q_{\text{max}} / (m_\ell + m'_\ell)^2]$  [17, 32], where  $G_F$  is the Fermi constant.

This EPA method overestimates the cross sections of the dielectron trident but is a good approximation for the coherent contribution to dimuon tridents [18, 25]. Ref. [18] establishes that EPA is generally not valid for tridents in regions where the virtual photon contributions are considerable. More relevant to our study, we note that the EPA will *underestimate* the cross section for tau tridents due to the larger contribution from off-shell photons.

Our cross section results are shown in Fig. 2 for the three benchmark nuclei. We calculate the full  $2 \rightarrow 4$  scattering calculation using the formalism described in Refs. [18, 19]. Here we include both coherent (solid) and incoherent (dashed) neutrino scattering off nuclei. Following the methodology of Ref. [19], we estimate the cross section uncertainties for coherent (incoherent) scattering as follows. We assume a 1% (3%) uncertainty for the nuclear (nucleon) form factors. Higher order QED corrections scale as  $\sim Z\alpha_{\text{EM}}/4\pi$ ; we assume a conservative 3% (3%) uncertainty for Argon, 6% (3%) uncertainty for Tungsten and 4% (3%) uncertainty for Iron. Our choice of weak mixing angle,  $\sin^2 \theta_W = 0.23129$ , also leads to a 5% (5%) uncertainty. Additionally, given our simplified nuclear model of a Fermi gas, we include a conservative 30% uncertainty for incoherent scattering. We add all our uncertainties in quadrature to get a total estimated uncertainty of 6% (31%) for Argon, 8% (31%) for Tungsten, and 6% (31%) for Iron. For further details, see

Ref. [19].

Due to lower neutrino energy threshold (see Table I), the coherent contribution dominates the trident cross section at low neutrino energies. This is clearly evident for the tau trident processes for which there is a larger separation in the energy thresholds between the coherent and incoherent processes. As the neutrino energy increases, the minimum photon momentum-transfer,  $Q^2$ , necessary to generate the final state will decrease. As  $Q^2$  increases, the nuclear form factor decreases and the hadronic form factors come to dominate as the neutrino can resolve more of the nuclear structure (see Fig. 5 and 6 in Appendix A). This leads to an initial crossing point where the cross section is dominated first by the coherent scattering and then by incoherent. For larger incoming neutrino energies, the contribution from coherent scattering is proportional to  $Z^2$  (where  $Z$  is the atomic number), and the contribution from incoherent scattering scales with the number nucleons, i.e. proportional to  $\sim 2Z$ . As the neutrino energy increases further, the enhancement from  $Z^2$  dependence of the coherent scattering will come to again dominate the  $2Z$  evolution of the incoherent piece, leading to a second crossing. This is most prominent for the tau trident processes in Fig. 2.

These two crossings are more pronounced in the tau trident case because they occur at much larger and more distinct neutrino energies. This is because of the presence of the tau, whose mass influences the momentum transfer  $Q^2$ . This pushes the crossing points to occur at larger neutrino energies and, therefore, there is a considerable region of energies sampled by the DUNE flux where incoherent production dominates the tau trident. We see from Fig 2 that coherent scattering dominates the muon trident much more rapidly as evolved with  $E_\nu$ .

### III. NEUTRINO TRIDENTS AT DUNE

The DUNE experiment [1] involves the production of an intense muon-neutrino beam from impinging 120 GeV proton beams on a graphite target, and placing detectors both near and far from the beam origin. These  $\nu_\mu$ 's with energies ranging up to several GeVs will then travel along the beamline and either interact with the detector or oscillate to other neutrino flavors. The posited length  $L = 574$  m between the beam origin and the ND is not sufficient for  $\nu_\tau$  production via standard neutrino oscillations for GeV-energy neutrinos. Although heavy charmed meson ( $D$ ,  $D_s$ ) decays could directly give  $\nu_\tau$ 's, their production rate is expected to be very small for a 120 GeV proton beam. While the observation of a signal consistent with the presence of  $\nu_\tau$  is often considered 'anomalous' and a prime target for BSM searches [12, 27, 33–38], neutrino tridents can be a significant source of tau leptons in the near detector, as we will see now.

With the trident cross sections calculated above, we obtain the expected number of events at an accelera-

tor neutrino experiment following the methodology of Ref. [19]:

$$N_{\text{trident}} = \Phi \sigma_{\text{conv}} \frac{M_{\text{det}}}{M} N_{\text{POT}}, \quad (5)$$

where  $N_{\text{POT}}$  is the number of protons on target,  $\Phi$  is the relevant integrated neutrino (or antineutrino) flux,  $M_{\text{det}}$  is the detector mass,  $M$  is the nuclear mass, and  $\sigma_{\text{conv}}$  is the cross section convoluted with the normalized neutrino flux:

$$\sigma_{\text{conv}} = \int \frac{1}{\Phi} \frac{d\Phi}{dE_\nu} \sigma_{\nu X} dE_\nu. \quad (6)$$

The relevant neutrino fluxes at various detectors considered here can be found in Appendix B. For DUNE, we consider the standard neutrino flux, as well as the tau-optimized configuration with more energetic neutrinos [30, 39].

In Fig. 3, we show the number of trident events, for all  $\nu_\mu$ -initiated tau tridents as well as  $\nu_\mu \rightarrow \nu_\mu \mu^+ \mu^-$  and  $\nu_e \rightarrow \nu_\tau \tau^+ e^-$ , at DUNE ND with 67 ton of Argon and  $3.3 \times 10^{21}$  POT in the forward horn current, or neutrino mode (see Appendix C for antineutrino mode). The uncertainties shown come from the cross section uncertainties outlined in Sec. II. For simplicity, we do not take into account uncertainties in the neutrino fluxes, which can in principle be reduced with other measurements (e.g., neutrino-electron scattering) at DUNE ND. Since experimentally one may be able to distinguish between coherent and incoherent scattering by observing the hadronic activity, we show their corresponding number of events separately. For the ease of cross check with previous literature [18, 19], we report the dimuon trident events as well, although our main focus is on the taus. For instance, our event numbers for the dimuon tridents roughly match with those given in Ref. [19], after taking into account the differences in the flux and detector mass used there from the older DUNE configuration. As for the tau tridents, in total, we expect  $4.11 \pm 1.17$  ( $0.97 \pm 0.28$ ) events in the standard mode and  $19.74 \pm 5.67$  ( $1.15 \pm 0.34$ ) events in the tau-optimized mode for the  $\nu_\mu \rightarrow \nu_\tau \tau^+ \mu^-$  ( $\bar{\nu}_\mu \rightarrow \bar{\nu}_\tau \tau^- \mu^+$ ) trident. Most of these events come from incoherent scattering due to DUNE's energy spectrum. This is in sharp contrast with the dimuon trident, where the coherent contribution is the dominant one. The tau-optimized mode gives more events because the flux peaks at higher energies, making it easier to pass the energy threshold for the tau tridents. For ditau tridents, we expect less than one event even in the tau-optimized mode. For completeness, we also report the numbers for  $\nu_e \rightarrow \nu_\tau \tau^+ e^-$  and  $\nu_\mu \rightarrow \nu_\mu \tau^+ \tau^-$  as well as their antineutrino counterparts in Fig. 3.

In Appendix C, we also show the number of trident events for FASER $\nu$ , T2K INGRID near detector, MINOS/MINOS+.



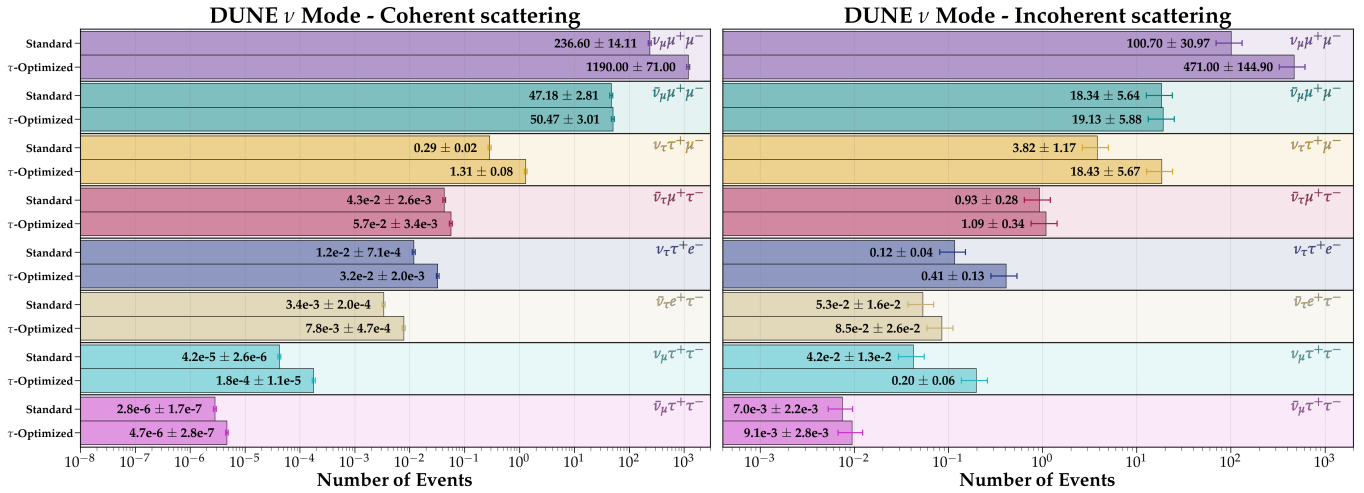


FIG. 3. Number of trident events from coherent (left) and incoherent (right) scattering at DUNE near detector with 67 ton of Argon and  $3.3 \times 10^{21}$  POT in the forward horn current mode for both standard and tau-optimized fluxes.

#### IV. TAU IDENTIFICATION FROM TRIDENTS AT DUNE

Detecting tau leptons in a realistic neutrino experimental setup like DUNE is notoriously challenging. First of all, LArTPCs cannot identify taus on an event-by-event basis due to the very short displaced vertex. Besides, the tau production cross section, either from intrinsic beam  $\nu_\tau$  or tridents, is very low, making virtually any experimental setup statistics-limited for tau observation. Tau reconstruction suffers from large backgrounds induced by the copious beam  $\nu_\mu$  component. Misreconstruction of final state particles could significantly degrade the signal-to-background ratio. This has been considered a major challenge in  $\nu_\tau$  detection at DUNE in the context of BSM studies [35–37, 40]. However, recent developments based on advanced machine-learning algorithms hold some promise [41–44].

The basic idea is to separate the tau signal events from backgrounds using kinematic differences, similar to those used in NOMAD [45]. Reference [44] ranked six kinematic variables providing the highest signal-to-background for tau reconstruction. The ratio of the transverse momenta,  $R_{\text{Miss}}^T = p_{\text{Miss}}^T / (p_{\text{Miss}}^T + p_\mu^T)$ , was identified as the rank-1 discriminator. Note that  $p_{\text{Miss}}^T$  is inferred from the total visible transverse momentum, including the muon, charged and neutral pions from tau decays, and possibly protons in the case of incoherent scattering. This ratio  $R_{\text{Miss}}^T$  is particularly relevant for our tau trident signal which always comes with additional missing energy from neutrinos, and therefore, we expect a larger  $R_{\text{Miss}}^T$  for the signal compared to the background.

In Fig. 4, we show the  $R_{\text{Miss}}^T$  distributions for the  $\mu\tau$  trident with incoherent (left) and coherent (right) contributions in blue for two benchmark average neutrino energies derived from their event distributions (see Fig. 12 in Appendix D). Here we consider the hadronic decays

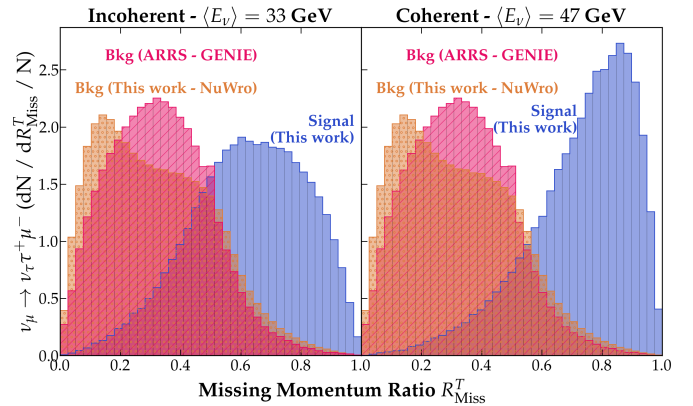


FIG. 4. Missing transverse momentum ratio distributions for the  $\nu_\mu \rightarrow \mu^- \nu_\tau \tau^+ \rightarrow \mu^- \nu_\tau \bar{\nu}_\tau + \text{hadrons}$ . The incoherent and coherent contributions are shown separately in the left and right panels, respectively, for two benchmark neutrino energies corresponding to the peak in DUNE event spectra for neutrino mode. The dominant  $\nu_\mu$  CC background labeled Aurisano-Rajaolisoa-Razafinime-Sousa (ARRS) is extracted from Ref. [44] (see also Refs. [42, 43]).

of tau, due to their larger branching ratio (65%), compared to the leptonic decays (17%–18%). We have simulated the hadronic tau decays using PYTHIA 8.3 [46]. For comparison, we show the dominant background from  $\nu_\mu$  CC extracted from the works of Aurisano-Rajaolisoa-Razafinime-Sousa (ARRS) [41–44], which used the GENIE event generator [47]. We also have generated the same background using the NuWro event generator [48]. Although the GENIE and NuWro distributions differ by  $\sim 20\%$ , they both shrink at larger  $R_{\text{Miss}}^T$  where most of the signal is. While not a full analysis, this serves to illustrate the point that discriminators like  $R_{\text{Miss}}^T$  could mitigate the large  $\nu_\mu$  CC background, enhance the signal-to-background ratio, and thus potentially allow us to ob-

serve the handful of tau trident events at DUNE ND. A detailed experimental feasibility study is left as future work.

For completeness, we also present the tau trident event rates for MINOS/MINOS+, T2K INGRID and FASER $\nu$ /FASER $\nu$ 2 in Appendix C.

## V. CONCLUSIONS

The neutrino trident process provides an important precision test of the SM electroweak interactions as well as a powerful probe for BSM physics. The next-generation accelerator neutrino experiment DUNE is in an excellent position to observe these rare SM processes for the first time. Among all trident channels, those involving tau leptons are particularly interesting, because any potential appearance of tau leptons at DUNE ND has been associated with BSM physics in the literature. Therefore, it is of paramount importance to delineate all potential SM backgrounds for tau events.

In this paper, we have identified one such SM source of tau lepton production at DUNE ND, namely, tau tridents. To this effect, we performed for the first time a detailed study of tau tridents at DUNE ND, and contrary to the common lore, found that they could yield a non-negligible event rate, especially with the tau-optimized flux configuration. We calculated the tau trident cross

section using the full  $2 \rightarrow 4$  scattering in order to obtain an accurate prediction of the event rate – significantly higher than the cross section calculated with the equivalent photon approximation. We found an intricate interplay between coherent and incoherent scattering which is distinct for tau tridents from electron and muon tridents. Lastly, we have identified a promising venue to enhance the poor signal-to-background ratio using kinematic variables, potentially leading to the observability of tau tridents for the first time at the DUNE experiment. We hope that these findings will motivate a dedicated experimental feasibility study of tau tridents at accelerator neutrino facilities.

## ACKNOWLEDGMENTS

We would like to thank Wolfgang Altmannshofer and Bei Zhou for useful discussions. We also thank Toni Mäkelä and Sebastian Trojanowski for useful correspondence on the FASER $\nu$  trident analysis. This manuscript has been authored in part by Fermi Research Alliance, LLC under Contract No. DE-AC02-07CH11359 with the U.S. Department of Energy, Office of Science, Office of High Energy Physics. This work of BD was partly supported by the U.S. Department of Energy under grant No. DE-SC 0017987. DLG is supported by an MCSS Graduate Fellowship.

## Appendix A: Form Factors

Here we give the expressions for the dimensionless flux factors  $h_X^{L/T}$  appearing in Eq. (2). In the coherent regime, these have the form [18]

$$h_c^T(Q^2, \hat{s}) = 8Z^2 e^2 \left( 1 - \frac{\hat{s}}{2E_\nu M} - \frac{\hat{s}^2}{4E_\nu^2 Q^2} \right) |F(Q^2)|^2, \quad (\text{A1})$$

$$h_c^L(Q^2, \hat{s}) = 4Z^2 e^2 \left( 1 - \frac{\hat{s}}{4E_\nu M} \right)^2 |F(Q^2)|^2, \quad (\text{A2})$$

where  $E_\nu$  is the incoming neutrino energy and  $M$  is the nuclear mass.  $F(Q^2)$  is the nuclear form factor. For argon and iron we have used

$$F(Q^2) = \int dr r^2 \frac{\sin(Qr)}{Qr} \rho(r), \quad (\text{A3})$$

where  $\rho$  is the spherically symmetric charge distribution of the nucleus, normalized as

$$\int dr r^2 \rho(r) = 1, \quad (\text{A4})$$

such that  $F(0) = 1$ . We rely on the nuclear charge density distributions fitted to elastic electron scattering data [49]. More specifically, we use the three-parameter Fermi charge distributions from Ref. [49].

For tungsten, we use the Woods-Saxon form factor [50–52]

$$F(Q^2) = \frac{1}{\int d^3r \rho(r)} \int d^3r \rho(r) \exp(-i\vec{q} \cdot \vec{r}), \quad (\text{A5})$$

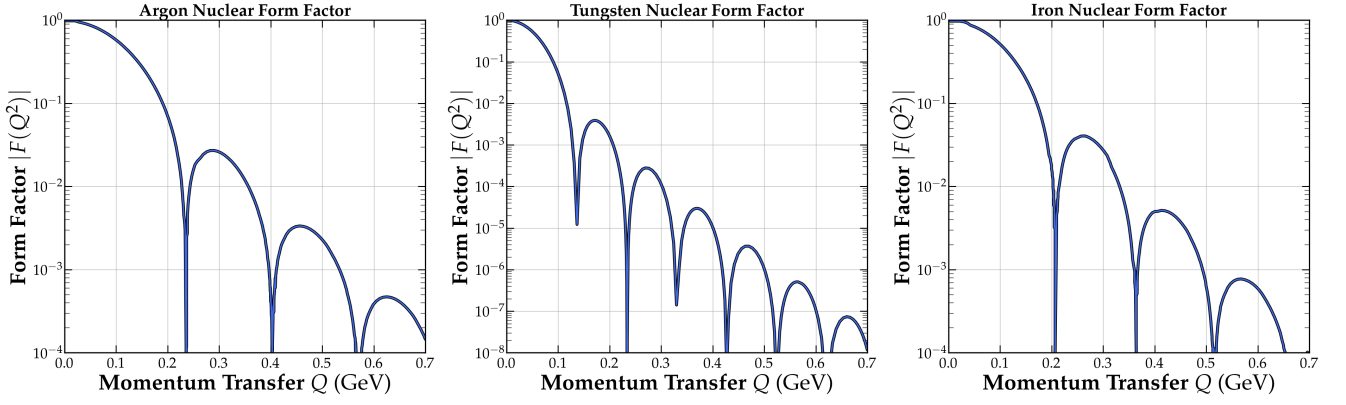


FIG. 5. Nuclear form factors for Argon (left), Tungsten (middle) and Iron (right).

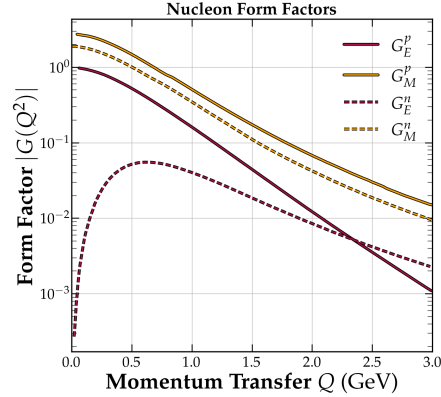


FIG. 6. Electric and magnetic form factors of the proton and neutron.

where the charge distribution follows the functional form

$$\rho(r) = \frac{\mathcal{N}}{1 + \exp\left(\frac{r-r_0}{\sigma_0}\right)}, \quad (\text{A6})$$

with  $r_0 = 1.126 \text{ fm } A^{1/3}$  and  $\sigma_0 = 0.523 \text{ fm}$ . Here  $\mathcal{N}$  is a normalization factor that is determined from the condition in Eq. (A4). This form factor can be expressed analytically using a symmetrized Fermi function as outlined in Ref. [18],

$$F(Q^2) = \frac{3\pi\sigma_0}{r_0^2 + \pi^2\sigma_0^2} \frac{\pi\sigma_0 \coth(\pi Q\sigma_0) \sin(Qr_0) - r_0 \cos(Qr_0)}{Qr_0 \sinh(\pi Q\sigma_0)}. \quad (\text{A7})$$

This is the final functional form used in the calculation of the tungsten form factor.

In Fig. 5, we show the nuclear form factors for argon, tungsten and iron. It is clear that all of them drop sharply as the momentum transfer increases, which is expected for coherent scattering.

In the incoherent (diffractive) regime, the flux factors appearing in Eq. (2) have the form [18]

$$h_i^T(Q^2, \hat{s}) = 8e^2 \left[ \left(1 - \frac{\hat{s}}{2E_\nu M_N} - \frac{\hat{s}^2}{4E_\nu^2 Q^2}\right) H_1^N(Q^2) + \frac{\hat{s}^2}{8E_\nu^2 M_N^2} H_2^N(Q^2) \right], \quad (\text{A8})$$

$$h_i^L(Q^2, \hat{s}) = 4e^2 \left[ \left(1 - \frac{\hat{s}}{4E_\nu M_N}\right)^2 H_1^N(Q^2) - \frac{\hat{s}^2}{16E_\nu^2 M_N^2} H_2^N(Q^2) \right], \quad (\text{A9})$$

where  $M_N = m_{p,n}$  is the proton or neutron mass, and  $H_{1/2}^N(Q^2)$  are the nucleon form factors, defined as [18]

$$H_1^N(Q^2) = |F_1^N(Q^2)|^2 - \tau |F_2^N(Q^2)|^2, \quad (\text{A10})$$

$$H_2^N(Q^2) = |F_1^N(Q^2) + F_2^N(Q^2)|^2, \quad (\text{A11})$$

where  $\tau = -Q^2/4M^2$ . The functions  $F_1^N(Q^2)$  and  $F_2^N(Q^2)$  here can be related to the electric and magnetic form-factors of the nucleons as

$$G_E^N(Q^2) = F_1^N + \tau F_2^N(Q^2), \quad (\text{A12})$$

$$G_M^N(Q^2) = F_1^N + F_2^N(Q^2). \quad (\text{A13})$$

While Ref. [18] utilizes a simple dipole parameterization for  $G_{E,M}^N(Q^2)$ , we utilize those from Ref. [53] (see also Ref. [54] for a recent reevaluation). The proton form factors were obtained from fits to the electron-proton elastic scattering cross section and polarization transfer measurements. The neutron form factors were obtained from fits to electron-nucleus (mostly  $^2\text{H}$  and  $^3\text{He}$ ) scattering data. Our results for the electric and magnetic form factors are shown in Fig. 6. Note that the electric form factor of the neutron goes to zero only at zero momentum transfer, whereas in the simple dipole approximation, it vanishes for all  $Q$  values.

## Appendix B: Neutrino Fluxes

In Fig. 7, we present the neutrino fluxes at the accelerator neutrino experiments considered here. For DUNE, we show the standard CP-optimized (solid) and tau-optimized (dashed) fluxes for the forward horn current polarity (neutrino) mode on top left panel and antineutrino mode on top right panel from Ref. [30]. Here we consider both electron and muon neutrino (and antineutrino) fluxes at the ND, but the muon neutrino fluxes are orders of magnitude larger. The MINOS (solid) and MINOS+ (dashed) fluxes for neutrino (middle left) and the MINOS flux for antineutrino (middle right) mode are taken from Refs. [55, 56]. Note that MINOS+ did not run in antineutrino mode. The T2K INGRID near detector fluxes (bottom left) are taken from Ref. [57]. Note that these fluxes are the same in T2K Phase-1 and Phase-2. We do not consider  $\text{NO}\nu\text{A}$  here, because the  $\text{NO}\nu\text{A}$  ND neutrino fluxes peak at slightly lower energies than the MINOS flux,  $E_\nu^{\text{peak}} \approx 2$  GeV [58], which is below the threshold for tau trident production (see Table I).

As for collider neutrino experiments, we take  $\text{FASER}\nu/\text{FASER}\nu 2$  as a prototypical example. The  $\nu_\mu + \bar{\nu}_\mu$  fluxes shown here (bottom right) are taken from Ref. [59].

## Appendix C: Trident Events at Other Accelerator/Collider Neutrino Experiments

Figure 3 in the main text showed the number of trident events at DUNE ND in the neutrino mode. Figure 8 shows the number of events in the antineutrino mode with the same 67 tons of detector mass and  $3.3 \times 10^{21}$  POT. The main reason for relegating this figure to the Appendix is that the tau-optimized mode, which gives the best event rate, may not have an antineutrino run at all, let alone for 3 years. Also, the number of trident events in the antineutrino mode are somewhat smaller than in the neutrino mode. This is due to lower fluxes (see Fig. 7), although the cross sections are the same for neutrinos and antineutrinos.

In Figs. 9 and 10, we show the trident event numbers at MINOS/MINOS+ and T2K INGRID detectors, respectively. The detector material is mostly Iron ( $^{56}\text{Fe}$ ) in both MINOS/MINOS+ and T2K. The MINOS ND has a fiducial mass of 28.6 ton and collected  $10.56 \times 10^{20}$  ( $3.36 \times 10^{20}$ ) POT in the neutrino (antineutrino) mode with the low-energy configuration of the NuMI beam having peak neutrino energy  $E_\nu^{\text{peak}} \approx 3$  GeV [60]. Therefore, the number of tau trident events is negligible, as can be seen from Fig. 9. MINOS+ ran with the same detector, but in the medium-energy configuration of NuMI, having  $E_\nu^{\text{peak}} \approx 7$  GeV and collecting  $9.69 \times 10^{20}$  POT in the neutrino mode [60]. MINOS+ did not run in antineutrino mode. Because of the higher  $E_\nu^{\text{peak}}$ , MINOS+ has slightly larger number of trident events than MINOS, but it is still negligible for the tau tridents due to relatively low POT. We do not include MINER $\nu\text{A}$  here, because although it collected similar POT as MINOS, its fiducial mass is only 8 ton, and therefore, the number of tau tridents will be smaller than the MINOS values.

At T2K, the on-axis near detector INGRID has a total fiducial mass of 99.4 t and collected  $3.9 \times 10^{21}$  POT in each neutrino and antineutrino modes in Phase-1. Phase-2 is expected to collect  $1.0 \times 10^{22}$  POT in each neutrino and antineutrino modes [61]. Although both POT and detector mass are larger for T2K, its flux only ranges from 0-4 GeV, and therefore, the number of tau tridents is even smaller than the MINOS case, as shown in Fig. 10.

We also consider collider neutrinos at  $\text{FASER}\nu/\text{FASER}\nu 2$  and calculate the number of trident events, as shown in Fig. 11. These numbers were not available for any of the trident channels until very recently [20, 21]. While Ref. [20] has no mention of tau tridents, Ref. [21] estimates those numbers to be small and experimentally challenging to probe. Our numbers corroborate this observation. Note that the neutrinos reaching  $\text{FASER}\nu$  are of much higher energy than the accelerator neutrinos, in the range of 10 GeV–1 TeV or so. Therefore, the coherent scattering will give the dominant contribution to the trident processes (see Fig. 2) at  $\text{FASER}\nu/\text{FASER}\nu 2$ . The  $\text{FASER}\nu$  detector



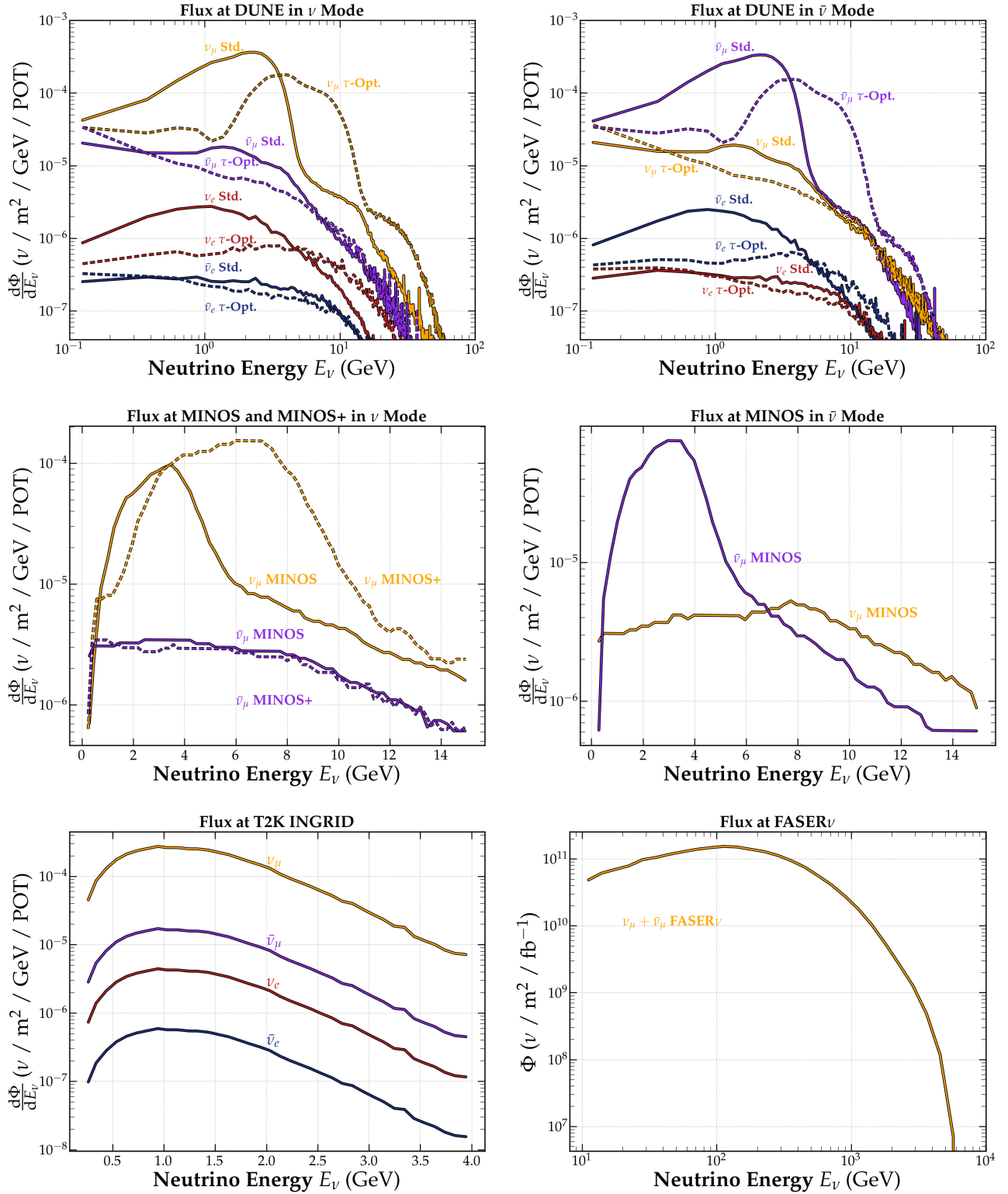


FIG. 7. Neutrino and antineutrino flux distributions for the accelerator neutrino experiments DUNE, MINOS/MINOS+, T2K considered here. Also shown (bottom right panel) is the collider neutrino flux at FASER $\nu$ . See text for details.

is made of tungsten ( $^{184}\text{W}$ ) and has a fiducial mass of 1.1 ton. FASER $\nu$  is expected to collect  $150 \text{ fb}^{-1}$  integrated luminosity during the current Run 3 of LHC. The proposed FASER $\nu$ 2 detector [62] will have a mass of 20 ton and

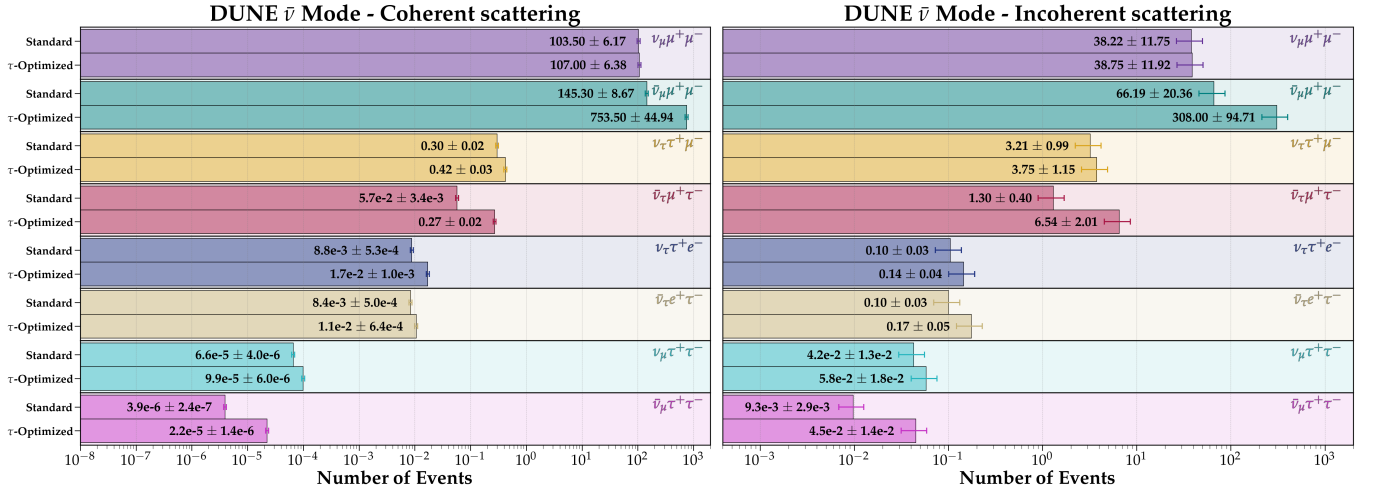


FIG. 8. Number of trident events from coherent (left) and incoherent (right) scattering at DUNE near detector with 67 ton of Argon and  $3.3 \times 10^{21}$  POT in antineutrino mode.

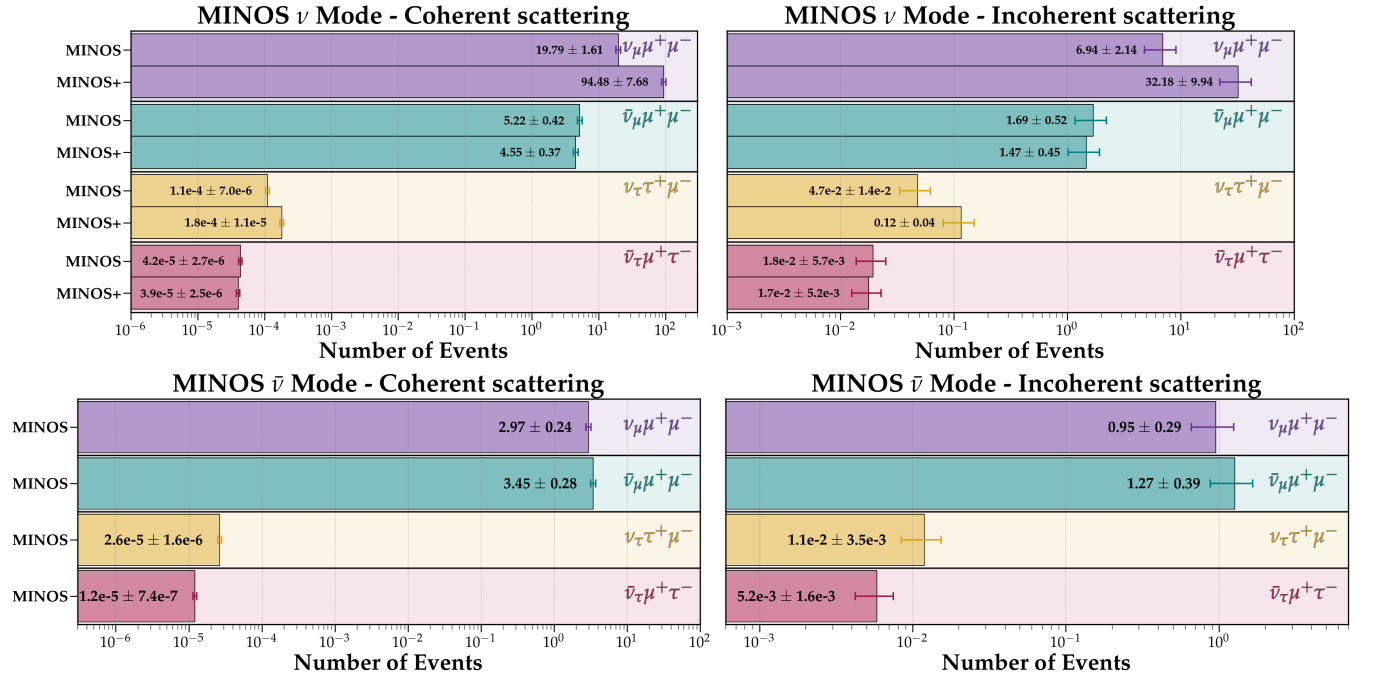


FIG. 9. Coherent (left) and incoherent (right) scattering events in the neutrino (top panels) and antineutrino (bottom panels) modes at MINOS and MINOS+ detectors with 28.6 ton Iron and  $10.56$  ( $9.69$ )  $\times 10^{20}$  POT for MINOS (MINOS+) in the neutrino mode and  $3.36 \times 10^{20}$  POT for MINOS in the antineutrino mode.

is expected to collect  $3 \text{ ab}^{-1}$  integrated luminosity at HL-LHC. In Fig. 11, we show the expected number of trident events at FASER $\nu$ /FASER $\nu 2$  with these configurations. Since the neutrino luminosities are readily available for FASER $\nu$ /FASER $\nu 2$ , we utilize a similar method as Eq. (5) but with the measured neutrino luminosity rather than  $N_{\text{POT}}$  to estimate the number of events. We find that while FASER $\nu$  will not have enough statistics to observe tau tridents, FASER $\nu 2$  will get about 20 events from coherent scattering and 6 from incoherent scattering. Although these numbers are similar to what we got for DUNE, there is a potentially large intrinsic  $\nu_\tau$  background of  $\mathcal{O}(2000)$  events [63–65] from decays of charmed mesons, which are copiously produced at the LHC energy. Therefore, we foresee that distinguishing  $\mathcal{O}(20)$  tau trident events from this large  $\nu_\tau$ -induced CC background will be quite challenging. In fact, this is going to be a general problem for other future collider neutrino experiments as well, such as SND@LHC [66], SND@SHiP [67] and FLArE [68].

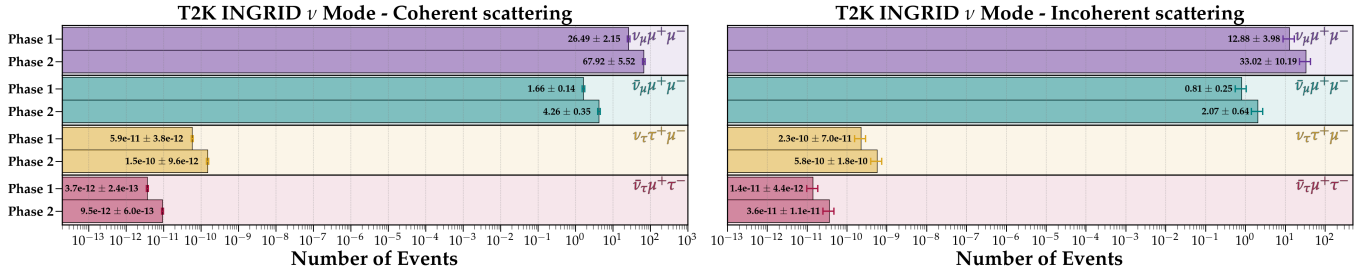


FIG. 10. Coherent (left) and incoherent (right) scattering events at T2K INGRID near detector with 99.4 ton of Iron and  $3.9(10) \times 10^{21}$  POT in Phase-1 (2).

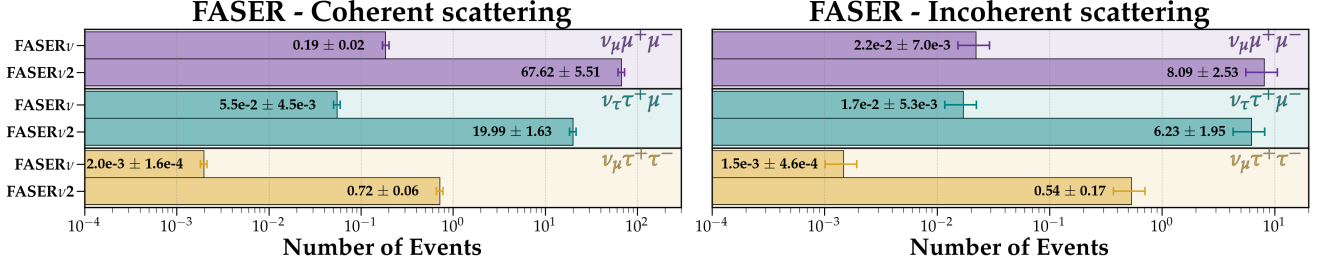


FIG. 11. Coherent (left) and incoherent (right) scattering events at FASERν and FASERν2 detectors with fiducial mass of 1.1 ton and 20 ton Tungsten, and integrated luminosity of  $150 \text{ fb}^{-1}$  and  $3 \text{ ab}^{-1}$ , respectively.

#### Appendix D: Tau Trident Event Distributions at DUNE

In Fig. 12, we show the number of events per bin as a function of neutrino energy  $E_\nu$  for the single-tau trident  $\nu_\mu N \rightarrow \nu_\tau N \tau^+ \mu^-$  with coherent (top) and incoherent (bottom) scatterings in DUNE neutrino (left) and antineutrino (right) beam mode for the standard (blue) and  $\nu_\tau$ -optimized (red) horn configurations. The average neutrino energy for each distribution is shown for reference, which is used for the missing momentum distribution in Fig. 4. Note that the peaks of these distributions occur at energies much higher than those at which the DUNE fluxes peak. This is simply because the trident processes involving tau leptons in the final state are phase-space suppressed and require a higher energy threshold. This is the main reason why the number of tau tridents is much smaller, as compared to the muon tridents.

- 
- [1] **DUNE** Collaboration, R. Acciarri *et al.*, “Long-Baseline Neutrino Facility (LBNF) and Deep Underground Neutrino Experiment (DUNE): Conceptual Design Report, Volume 2: The Physics Program for DUNE at LBNF,” [arXiv:1512.06148](#) [[physics.ins-det](#)].
  - [2] **Hyper-Kamiokande** Collaboration, K. Abe *et al.*, “Hyper-Kamiokande Design Report,” [arXiv:1805.04163](#) [[physics.ins-det](#)].
  - [3] **DONuT** Collaboration, K. Kodama *et al.*, “Final tau-neutrino results from the DONuT experiment,” *Phys. Rev. D* **78** (2008) 052002, [arXiv:0711.0728](#) [[hep-ex](#)].
  - [4] **OPERA** Collaboration, N. Agafonova *et al.*, “Final Results of the OPERA Experiment on  $\nu_\tau$  Appearance in the CNGS Neutrino Beam,” *Phys. Rev. Lett.* **120** no. 21, (2018) 211801, [arXiv:1804.04912](#) [[hep-ex](#)].
  - [5] W. Czyz, G. C. Sheppey, and J. D. Walecka, “Neutrino production of lepton pairs through the point four-fermion interaction,” *Nuovo Cim.* **34** (1964) 404–435.
  - [6] R. W. Brown, R. H. Hobbs, J. Smith, and N. Stanko, “Intermediate boson. iii. virtual-boson effects in neutrino trident production,” *Phys. Rev. D* **6** (1972) 3273–3292.
  - [7] W. Altmannshofer, S. Gori, M. Pospelov, and I. Yavin, “Neutrino Trident Production: A Powerful Probe of New Physics with Neutrino Beams,” *Phys. Rev. Lett.* **113** (2014) 091801, [arXiv:1406.2332](#) [[hep-ph](#)].
  - [8] G. Magill and R. Plestid, “Probing new charged scalars with neutrino trident production,” *Phys. Rev. D* **97** no. 5, (2018) 055003, [arXiv:1710.08431](#) [[hep-ph](#)].
  - [9] P. Ballett, M. Hostert, S. Pascoli, Y. F. Perez-Gonzalez, [Erratum: *Phys.Rev.Lett.* 121, 139901 (2018)].

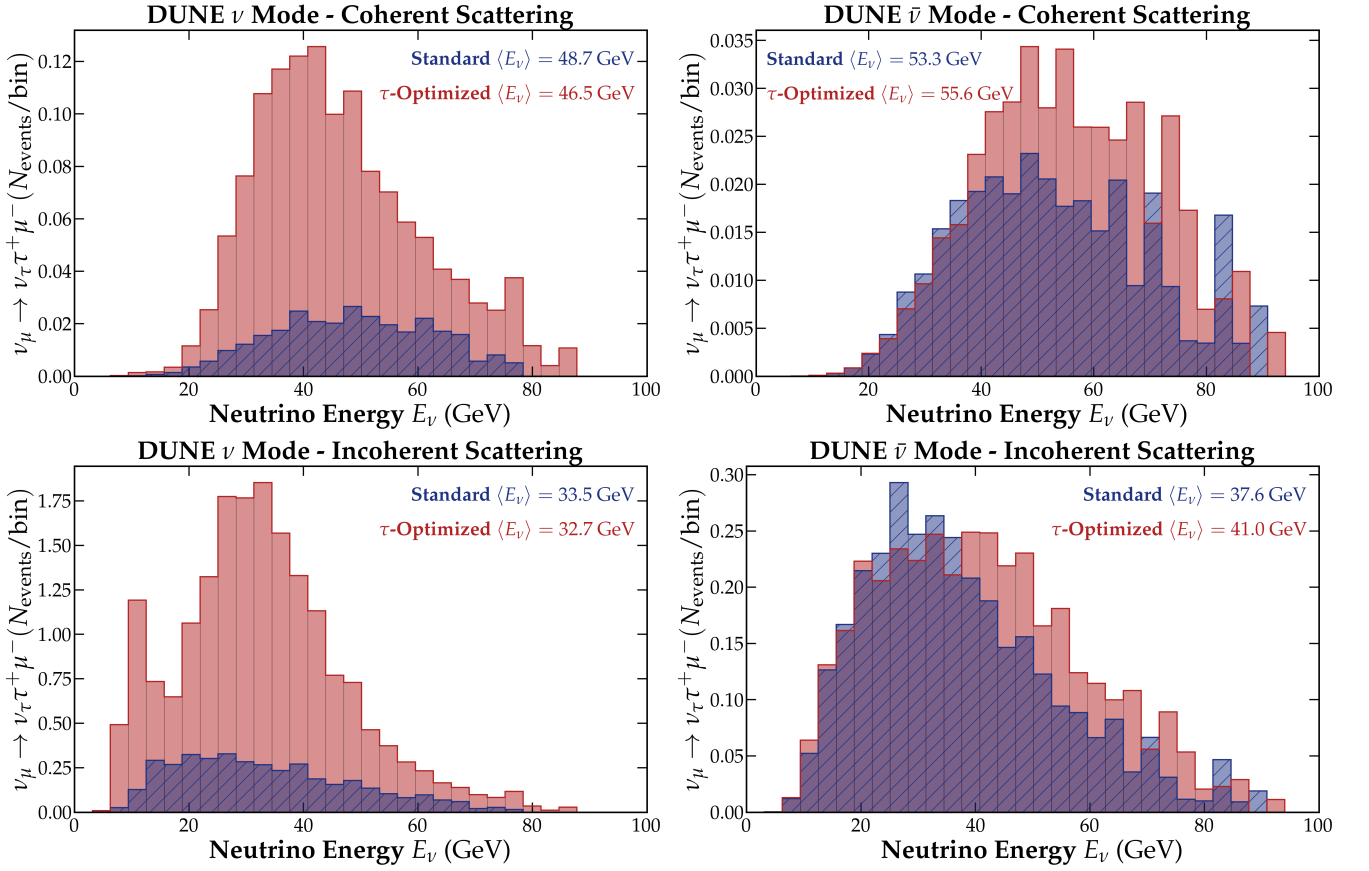


FIG. 12. Number of events per bin as a function of neutrino energy  $E_\nu$  for the single-tau trident  $\nu_\mu N \rightarrow \nu_\tau N \tau^+ \mu^-$  with coherent (top) and incoherent (bottom) scatterings in DUNE neutrino (left) and antineutrino (right) beam mode for the standard (blue) and tau-optimized (red) horn configurations. We have taken 67 ton fiducial mass ND and an exposure of  $3.3 \times 10^{21}$  POT.

- Z. Tabrizi, and R. Zukanovich Funchal, “Z’s in neutrino scattering at DUNE,” *Phys. Rev. D* **100** no. 5, (2019) 055012, [arXiv:1902.08579 \[hep-ph\]](#).
- [10] T. Shimomura and Y. Uesaka, “Kinematical distributions of coherent neutrino trident production in gauged  $L_\mu - L_\tau$  model,” *Phys. Rev. D* **103** no. 3, (2021) 035022, [arXiv:2009.13773 \[hep-ph\]](#).
- [11] Y. Cheng, X.-G. He, Z.-L. Huang, and M.-W. Li, “Type-II seesaw triplet scalar effects on neutrino trident scattering,” *Phys. Lett. B* **831** (2022) 137218, [arXiv:2204.05031 \[hep-ph\]](#).
- [12] I. Bigaran, X.-G. He, M. A. Schmidt, G. Valencia, and R. Volkas, “Lepton-flavor-violating tau decays from triality,” *Phys. Rev. D* **107** no. 5, (2023) 055001, [arXiv:2212.09760 \[hep-ph\]](#).
- [13] CHARM-II Collaboration, D. Geiregat *et al.*, “First observation of neutrino trident production,” *Phys. Lett. B* **245** (1990) 271–275.
- [14] CCFR Collaboration, S. R. Mishra *et al.*, “Neutrino Tridents and W Z Interference,” *Phys. Rev. Lett.* **66** (1991) 3117–3120.
- [15] NuTeV Collaboration, T. Adams *et al.*, “Neutrino trident production from NuTeV,” in *29th International Conference on High-Energy Physics*, pp. 631–634. 7, 1998. [arXiv:hep-ex/9811012](#).
- [16] NuTeV Collaboration, T. Adams *et al.*, “Evidence for diffractive charm production in muon-neutrino Fe and anti-muon-neutrino Fe scattering at the Tevatron,” *Phys. Rev. D* **61** (2000) 092001, [arXiv:hep-ex/9909041](#).
- [17] G. Magill and R. Plestid, “Neutrino Trident Production at the Intensity Frontier,” *Phys. Rev. D* **95** no. 7, (2017) 073004, [arXiv:1612.05642 \[hep-ph\]](#).
- [18] P. Ballett, M. Hostert, S. Pascoli, Y. F. Perez-Gonzalez, Z. Tabrizi, and R. Zukanovich Funchal, “Neutrino Trident Scattering at Near Detectors,” *JHEP* **01** (2019) 119, [arXiv:1807.10973 \[hep-ph\]](#).
- [19] W. Altmannshofer, S. Gori, J. Martín-Albo, A. Sousa, and M. Wallbank, “Neutrino Tridents at DUNE,” *Phys. Rev. D* **100** no. 11, (2019) 115029, [arXiv:1902.06765 \[hep-ph\]](#).
- [20] R. Francener, V. P. Goncalves, and D. R. Gratiere, “Neutrino trident scattering at the LHC energy regime,” [arXiv:2406.13593 \[hep-ph\]](#).
- [21] W. Altmannshofer, T. Mäkelä, S. Sarkar, S. Trojanowski, K. Xie, and B. Zhou, “Discovering neutrino tridents at the Large Hadron Collider,” [arXiv:2406.16803 \[hep-ph\]](#).
- [22] S.-F. Ge, M. Lindner, and W. Rodejohann, “Atmospheric Trident Production for Probing New Physics,” *Phys. Lett. B* **772** (2017) 164–168, [arXiv:1702.02617 \[hep-ph\]](#).
- [23] B. Zhou and J. F. Beacom, “W-boson and trident

- production in TeV–PeV neutrino observatories,” *Phys. Rev. D* **101** no. 3, (2020) 036010, [arXiv:1910.10720 \[hep-ph\]](#).
- [24] J. A. Formaggio and G. P. Zeller, “From eV to EeV: Neutrino Cross Sections Across Energy Scales,” *Rev. Mod. Phys.* **84** (2012) 1307–1341, [arXiv:1305.7513 \[hep-ex\]](#).
- [25] B. Zhou and J. F. Beacom, “Neutrino-nucleus cross sections for W-boson and trident production,” *Phys. Rev. D* **101** no. 3, (2020) 036011, [arXiv:1910.08090 \[hep-ph\]](#).
- [26] **FASEER** Collaboration, H. Abreu *et al.*, “Technical Proposal: FASERnu,” [arXiv:2001.03073 \[physics.ins-det\]](#).
- [27] P. Machado, H. Schulz, and J. Turner, “Tau neutrinos at DUNE: New strategies, new opportunities,” *Phys. Rev. D* **102** no. 5, (2020) 053010, [arXiv:2007.00015 \[hep-ph\]](#).
- [28] J. Isaacson, S. Höche, F. Siegert, and S. Wang, “Tau polarization and correlated decays in neutrino experiments,” *Phys. Rev. D* **108** no. 9, (2023) 093004, [arXiv:2303.08104 \[hep-ph\]](#).
- [29] **DUNE** Collaboration, V. Hewes *et al.*, “Deep Underground Neutrino Experiment (DUNE) Near Detector Conceptual Design Report,” *Instruments* **5** no. 4, (2021) 31, [arXiv:2103.13910 \[physics.ins-det\]](#).
- [30] L. Fields. <https://glaucus.crc.nd.edu/DUNEFluxes/>.
- [31] J. Lovseth and M. Radomski, “Kinematical distributions of neutrino-produced lepton triplets,” *Phys. Rev. D* **3** (1971) 2686–2706.
- [32] R. Belusevic and J. Smith, “W - Z Interference in Neutrino - Nucleus Scattering,” *Phys. Rev. D* **37** (1988) 2419.
- [33] P. Coloma, D. V. Forero, and S. J. Parke, “DUNE Sensitivities to the Mixing between Sterile and Tau Neutrinos,” *JHEP* **07** (2018) 079, [arXiv:1707.05348 \[hep-ph\]](#).
- [34] P. Bakhti, Y. Farzan, and M. Rajaei, “Secret interactions of neutrinos with light gauge boson at the DUNE near detector,” *Phys. Rev. D* **99** no. 5, (2019) 055019, [arXiv:1810.04441 \[hep-ph\]](#).
- [35] A. De Gouvêa, K. J. Kelly, G. V. Stenico, and P. Pasquini, “Physics with Beam Tau-Neutrino Appearance at DUNE,” *Phys. Rev. D* **100** no. 1, (2019) 016004, [arXiv:1904.07265 \[hep-ph\]](#).
- [36] A. Ghoshal, A. Giarnetti, and D. Meloni, “On the role of the  $\nu_\tau$  appearance in DUNE in constraining standard neutrino physics and beyond,” *JHEP* **12** (2019) 126, [arXiv:1906.06212 \[hep-ph\]](#).
- [37] P. Coloma, J. López-Pavón, S. Rosauero-Alcaraz, and S. Urrea, “New physics from oscillations at the DUNE near detector, and the role of systematic uncertainties,” *JHEP* **08** (2021) 065, [arXiv:2105.11466 \[hep-ph\]](#).
- [38] P. S. B. Dev, B. Dutta, T. Han, and D. Kim, “Anomalous tau neutrino appearance from light mediators in short-baseline neutrino experiments,” *Phys. Lett. B* **850** (2024) 138500, [arXiv:2304.02031 \[hep-ph\]](#).
- [39] **DUNE** Collaboration, B. Abi *et al.*, “Deep Underground Neutrino Experiment (DUNE), Far Detector Technical Design Report, Volume I Introduction to DUNE,” *JINST* **15** no. 08, (2020) T08008, [arXiv:2002.02967 \[physics.ins-det\]](#).
- [40] A. Giarnetti and D. Meloni, “Probing source and detector nonstandard interaction parameters at the DUNE near detector,” *Phys. Rev. D* **104** no. 1, (2021) 015027, [arXiv:2005.10272 \[hep-ph\]](#).
- [41] A. Aurisano, “Tau Neutrino Physics at DUNE,” 2021. <https://indico.cern.ch/event/855372/contributions/4441599/attachments/2305916/3922951/aurisanoNuTauPhysicsDUNE.pdf>.
- [42] M. Rajaoalisoa, “Search for anomalous tau neutrino appearance in the DUNE Near Detector,” 2021. [https://indico.bnl.gov/event/10495/contributions/53910/attachments/37406/61630/NuTau21\\_Search\\_for\\_anomalous\\_tau\\_neutrino\\_in\\_DUNE\\_ND.pdf](https://indico.bnl.gov/event/10495/contributions/53910/attachments/37406/61630/NuTau21_Search_for_anomalous_tau_neutrino_in_DUNE_ND.pdf).
- [43] S. H. Razafinime, “Studies of tau neutrino appearance at the DUNE Near Detector complex,” 2022. <https://indico.kps.or.kr/event/30/contributions/737/>.
- [44] A. Sousa, “Beyond Three-Flavor  $\nu$  Oscillations with DUNE,” 2022. [https://indico.fnal.gov/event/22303/contributions/244935/attachments/157422/205929/Sousa\\_DUNE\\_Beyond\\_3\\_flavor\\_Snowmass\\_July\\_19\\_2022.pdf](https://indico.fnal.gov/event/22303/contributions/244935/attachments/157422/205929/Sousa_DUNE_Beyond_3_flavor_Snowmass_July_19_2022.pdf).
- [45] **NOMAD** Collaboration, P. Astier *et al.*, “Final NOMAD results on muon-neutrino  $\rightarrow$  tau-neutrino and electron-neutrino  $\rightarrow$  tau-neutrino oscillations including a new search for tau-neutrino appearance using hadronic tau decays,” *Nucl. Phys. B* **611** (2001) 3–39, [arXiv:hep-ex/0106102](#).
- [46] C. Bierlich *et al.*, “A comprehensive guide to the physics and usage of PYTHIA 8.3” *SciPost Phys. Codeb.* **2022** (2022) 8, [arXiv:2203.11601 \[hep-ph\]](#).
- [47] C. Andreopoulos *et al.*, “The GENIE Neutrino Monte Carlo Generator,” *Nucl. Instrum. Meth. A* **614** (2010) 87–104, [arXiv:0905.2517 \[hep-ph\]](#).
- [48] T. Golan, J. T. Sobczyk, and J. Zmuda, “NuWro: the Wrocław Monte Carlo Generator of Neutrino Interactions,” *Nucl. Phys. B Proc. Suppl.* **229-232** (2012) 499–499.
- [49] H. De Vries, C. W. De Jager, and C. De Vries, “Nuclear charge and magnetization density distribution parameters from elastic electron scattering,” *Atom. Data Nucl. Data Tabl.* **36** (1987) 495–536.
- [50] R. D. Woods and D. S. Saxon, “Diffuse Surface Optical Model for Nucleon-Nuclei Scattering,” *Phys. Rev.* **95** (1954) 577–578.
- [51] G. Fricke, C. Bernhardt, K. Heilig, L. A. Schaller, L. Schellenberg, E. B. Shera, and C. W. de Jager, “Nuclear Ground State Charge Radii from Electromagnetic Interactions,” *Atom. Data Nucl. Data Tabl.* **60** (1995) 177–285.
- [52] U. D. Jentschura and V. G. Serbo, “Nuclear form factor, validity of the equivalent photon approximation and Coulomb corrections to muon pair production in photon-nucleus and nucleus-nucleus collisions,” *Eur. Phys. J. C* **64** (2009) 309–317, [arXiv:0908.3853 \[hep-ph\]](#).
- [53] W. M. Alberico, S. M. Bilenky, C. Giunti, and K. M. Graczyk, “Electromagnetic form factors of the nucleon: New Fit and analysis of uncertainties,” *Phys. Rev. C* **79** (2009) 065204, [arXiv:0812.3539 \[hep-ph\]](#).
- [54] Z. Ye, J. Arrington, R. J. Hill, and G. Lee, “Proton and Neutron Electromagnetic Form Factors and Uncertainties,” *Phys. Lett. B* **777** (2018) 8–15, [arXiv:1707.09063 \[nucl-ex\]](#).
- [55] **MINOS** Collaboration, P. Adamson *et al.*, “A Study of



- Muon Neutrino Disappearance Using the Fermilab Main Injector Neutrino Beam,” *Phys. Rev. D* **77** (2008) 072002, [arXiv:0711.0769 \[hep-ex\]](#).
- [56] **MINERvA** Collaboration, L. Aliaga *et al.*, “Neutrino Flux Predictions for the NuMI Beam,” *Phys. Rev. D* **94** no. 9, (2016) 092005, [arXiv:1607.00704 \[hep-ex\]](#). [Addendum: *Phys.Rev.D* 95, 039903 (2017)].
- [57] **T2K** Collaboration, K. Abe *et al.*, “Measurement of the muon neutrino inclusive charged-current cross section in the energy range of 1–3 GeV with the T2K INGRID detector,” *Phys. Rev. D* **93** no. 7, (2016) 072002, [arXiv:1509.06940 \[hep-ex\]](#).
- [58] K. K. Maan, H. Duyang, S. R. Mishra, and V. Bhatnagar, “Neutrino Flux Studies at NOvA,” in *Meeting of the APS Division of Particles and Fields*. 11, 2015. [arXiv:1511.00287 \[hep-ex\]](#).
- [59] **FASER** Collaboration, H. Abreu *et al.*, “Detecting and Studying High-Energy Collider Neutrinos with FASER at the LHC,” *Eur. Phys. J. C* **80** no. 1, (2020) 61, [arXiv:1908.02310 \[hep-ex\]](#).
- [60] A. Aurisano, “Recent Results from MINOS and MINOS+,” in *XXVIII International Conference on Neutrino Physics and Astrophysics*, p. 423. 2018.
- [61] **T2K** Collaboration, K. Abe *et al.*, “Sensitivity of the T2K accelerator-based neutrino experiment with an Extended run to  $20 \times 10^{21}$  POT,” [arXiv:1607.08004 \[hep-ex\]](#).
- [62] J. L. Feng *et al.*, “The Forward Physics Facility at the High-Luminosity LHC,” *J. Phys. G* **50** no. 3, (2023) 030501, [arXiv:2203.05090 \[hep-ex\]](#).
- [63] W. Bai, M. Diwan, M. V. Garzelli, Y. S. Jeong, F. K. Kumar, and M. H. Reno, “Parton distribution function uncertainties in theoretical predictions for far-forward tau neutrinos at the Large Hadron Collider,” *JHEP* **06** (2022) 148, [arXiv:2112.11605 \[hep-ph\]](#).
- [64] W. Bai, M. V. Diwan, M. V. Garzelli, Y. S. Jeong, K. Kumar, and M. H. Reno, “Prompt electron and tau neutrinos and antineutrinos in the forward region at the LHC,” *JHEAp* **34** (2022) 212–216, [arXiv:2203.07212 \[hep-ph\]](#).
- [65] M. H. Reno, “Neutrinos at a forward physics facility.” <https://indico.sanfordlab.org/event/53/contributions/860/attachments/514/1278/CETUP2023-Reno.pdf>. Talk at CETUP\* 2023.
- [66] **SND@LHC** Collaboration, G. Acampora *et al.*, “SND@LHC: the scattering and neutrino detector at the LHC,” *JINST* **19** no. 05, (2024) P05067, [arXiv:2210.02784 \[hep-ex\]](#).
- [67] **SHiP** Collaboration, M. Anelli *et al.*, “A facility to Search for Hidden Particles (SHiP) at the CERN SPS,” [arXiv:1504.04956 \[physics.ins-det\]](#).
- [68] B. Batell, J. L. Feng, and S. Trojanowski, “Detecting Dark Matter with Far-Forward Emulsion and Liquid Argon Detectors at the LHC,” *Phys. Rev. D* **103** no. 7, (2021) 075023, [arXiv:2101.10338 \[hep-ph\]](#).